

This work was written as part of one of the author's official duties as an Employee of the United States Government and is therefore a work of the United States Government. In accordance with 17 U.S.C. 105, no copyright protection is available for such works under U.S. Law.

Public Domain Mark 1.0

<https://creativecommons.org/publicdomain/mark/1.0/>

Access to this work was provided by the University of Maryland, Baltimore County (UMBC) ScholarWorks@UMBC digital repository on the Maryland Shared Open Access (MD-SOAR) platform.

Please provide feedback

Please support the ScholarWorks@UMBC repository by emailing scholarworks-group@umbc.edu and telling us what having access to this work means to you and why it's important to you. Thank you.

Detection of volcanic ash clouds from Nimbus 7/total ozone mapping spectrometer

C. J. Seftor,¹ N. C. Hsu,¹ J. R. Herman,² P. K. Bhartia,²
O. Torres,¹ W. I. Rose,³ D. J. Schneider,³ and N. Krotkov¹

Abstract. Measured radiances from the Version 7 reprocessing of the Nimbus 7/total ozone mapping spectrometer (TOMS) 340- and 380-nm channels are used to detect absorbing particulates injected into the atmosphere after the El Chichon eruption on April 4, 1982. It is shown that while the single-channel reflectivity determined from the 380-nm channel is able to detect clouds and haze composed of nonabsorbing aerosols, the spectral contrast between the 340- and 380-nm channels is sensitive to absorbing particulates such as volcanic ash, desert dust, or smoke from biomass burning. In this paper the spectral contrast between these two channels is used to detect the volcanic ash injection into the atmosphere and to track its evolution for several days. The movement of the ash clouds is shown to be consistent with the motions expected from the National Centers for Environmental Prediction (NCEP)-derived balanced wind fields in the troposphere and lower stratosphere. The movement of the volcanic SO₂ cloud detected from TOMS data was also in agreement with the NCEP wind at higher altitudes of up to 100–10 mbar. The vertical wind shear in the neighborhood of the eruption site resulted in a clear separation of the ash and SO₂ clouds. The location and movement of the ash cloud are consistent with information obtained by the advanced very high resolution radiometer (AVHRR) instrument on board the NOAA 7 satellite and to ground reports of ash fall.

1. Introduction

Atmospheric radiance information from the Version 7 Nimbus 7 and Meteor 3 total ozone mapping spectrometer (TOMS) data sets has been used to generate a 16-year record of ozone changes. Of the six wavelength channels available on these instruments, the three that are insensitive to the amount of ozone in the atmosphere (340, 360, and 380 nm) can be used to determine the effective reflectivity of the lower boundary, R_λ . R_λ can be determined by comparing the measured upwelling radiance to the atmospheric backscattering from a pure Rayleigh atmosphere over a Lambertian surface. If clouds are present, two different Lambertian surfaces are assumed, one representing the ground and one representing clouds. The calculated reflectivity using the 380-nm channel radiance is a measure of the presence of clouds, haze, or a reflective ground surface such as snow or ice. The recalibration of Nimbus 7/TOMS in the Version 7 data set permits the wavelength dependence of the effective reflectivities to be calculated with an accuracy of about 0.1% and the absolute reflectivities to be calculated to better than 1%. Details of the algorithm used to generate the Version 7 data sets are given by *McPeters et al.* [1996]. Details of the Version 7 calibration of the Nimbus-7 TOMS instrument are given by *Wellemeyer et al.* [1996] and of the Meteor 3 TOMS instrument are given by *Seftor et al.* [1997].

On the basis of radiative transfer calculations in a Rayleigh scattering atmosphere, the presence of aerosols changes the spectral dependence in the radiances. Depending on the characteristics of the aerosols, they can be either absorbing or nonabsorbing in the UV spectral region [*D'Almeida*, 1987; *Patterson*, 1981; *Patterson et al.*, 1983; *Patterson and McMahon*, 1984]. The spectral dependence is most pronounced for UV-absorbing aerosols, which cause R_λ to increase with wavelength. While the ozone retrieval algorithm is designed to minimize the spectral dependence from clouds, other types of nonabsorbing aerosols, under certain conditions, can cause R_λ to decrease with wavelength. TOMS data can therefore be used to clearly distinguish between absorbing particulates (e.g., smoke from biomass burning, desert dust, and volcanic ash) and nonabsorbing particulates (e.g., water clouds, haze, and volcanic H₂SO₄ aerosols).

In practice, the spectral contrast is measured and tracked through a quantity known as the aerosol index:

$$A = -100 \log_{10} \left(\frac{I_{340}}{I_{380}} \right)_{\text{meas}} + 100 \log_{10} \left(\frac{I_{340}}{I_{380}} \right)_{\text{calc}}, \quad (1)$$

where $(I_{340}/I_{380})_{\text{meas}}$ is the measured spectral contrast between the 340- and 380-nm radiances and $(I_{340}/I_{380})_{\text{calc}}$ is the spectral contrast between the 340- and 380-nm radiances calculated using a Rayleigh scattering atmosphere and reflectivity determined from the 380-nm channel.

Since the effective reflectivity is determined by requiring $(I_{380})_{\text{meas}} = (I_{380})_{\text{calc}}$,

$$A = -100 \log_{10} [(I_{340})_{\text{meas}}/(I_{340})_{\text{calc}}]. \quad (2)$$

Without additional information about the absorbing particulates observed in the TOMS data (e.g., the refractive index and particle size distribution), the aerosol index can be used to

¹Hughes STX Corporation, Greenbelt, Maryland.

²NASA Goddard Space Flight Center, Greenbelt, Maryland.

³Department of Geological Engineering and Sciences, Michigan Technological University, Houghton.

determine their location and the relative amount of particulate matter [Herman *et al.*, 1997].

This paper is one of a series of papers reporting on the ability of TOMS instruments to detect tropospheric aerosols. Previous papers have described using TOMS data to detect biomass burning [Hsu *et al.*, 1996] and map the global distribution of UV-absorbing aerosols [Herman *et al.*, 1997]. Subsequent papers will detail the theoretical radiative transfer aspects of detecting tropospheric and volcanic aerosols at TOMS wavelengths.

In this paper the detection of volcanic ash is demonstrated by looking at the April 4, 1982, eruptions of El Chichon. The development of the ash cloud is mapped and its motion is followed. Since the TOMS wavelength channels can also be used to derive the total column amount and geographical distribution of SO₂ in the atmosphere [Krueger *et al.*, 1995], comparisons are made between the motion of the ash cloud and the SO₂ cloud. The ash cloud motions are confirmed from infrared satellite observations obtained by the NOAA 7 advanced very high resolution radiometer (AVHRR). Finally, in order to demonstrate the ability to determine optical depths from such data, a sample calculation is performed for April 6, 1982, from a radiative transfer model using aerosol parameters consistent with volcanic ash.

2. The El Chichon Eruption and Resulting SO₂ Cloud

Two of the El Chichon eruptions occurred on April 4, 1982, at 0135 and 1122 UT, respectively [Sigurdsson *et al.*, 1984]. These two eruptions (which, along with a smaller one on March 28) injected $7 (\pm 2) \times 10^9$ kg of SO₂ [Bluth *et al.*, 1992] to levels as high as 20–26 km in the atmosphere [Carey and Sigurdsson, 1986]. The SO₂ effects were significant for a period of a few weeks and then decreased as the SO₂ became converted into H₂SO₄. The H₂SO₄ aerosol persisted in the stratosphere and troposphere for several years before gradually fading back to pre-eruption amounts. This same phenomenon was also observed by TOMS after the Mount Pinatubo eruption in June 1991 [Torres *et al.*, 1995].

The ability to determine the presence of SO₂ from TOMS radiance measurements has long been known, and an algorithm designed to detect SO₂ was contained in previous versions of the TOMS processing system [Krueger, 1983]. For the Version 7 processing of TOMS data an improved algorithm to detect SO₂ was implemented. This algorithm routinely produces an index, called the sulfur dioxide index (SOI), which is related to the amount of SO₂ in the atmosphere. Radiative transfer studies indicate that the Version 7 SOI is an accurate measure of the amount of SO₂ for ash-free plumes in the atmosphere up to 100 Dobson units (DU) (with an SOI of 1 being equivalent to 1 DU). The SOI begins to lose some accuracy between 100 and 200 DU and becomes unreliable above 200 DU. The presence of ash causes the SOI to underestimate the amount of SO₂; the underestimation is proportional to the ash optical thickness. Details of the algorithm are given by *McPeters et al.* [1996]. For this work an upper limit of 200 was placed on the SOI, and it was used to determine the geographical location and extent of the SO₂ cloud.

The SO₂ cloud represented by the SOI for April 4 is shown in Figure 1a. The areal coverage ("footprint") of the TOMS measurements has been approximated by rectangles. TOMS is

a scanning instrument, and the size of the footprint and corresponding size of the rectangle increase with the scan angle.

Figures 1a–1d show the derived SO₂ cloud for four days, April 4, 5, 6, and 8 (data were missing on April 7) as TOMS passed overhead at local noon (1800 UT). Figure 1a shows that the initial SO₂ cloud covered an area extending east past the Yucatan Peninsula and west to the Atlantic Ocean. Winds derived from NCEP data indicate predominantly westerly winds in the troposphere and easterly winds in the stratosphere. The zonal spreading of the cloud indicates shearing of the vertical column of SO₂ by these winds. On April 5 and 6 the displacement of the SO₂ cloud was mainly toward the west and northwest, following the winds at roughly 10–30 mbar. These motions are comparable to those seen in other observations [Barth *et al.*, 1983] and in previous versions of the TOMS data [Krueger, 1983]. Krueger also indicated that the amount of SO₂ released into the atmosphere reached values higher than 700 DU; the upper limit of 200 placed on the SOI precludes a comparison with values obtained from the Version 7 algorithm.

3. The Ash Cloud

Ash from the eruption of El Chichon was seen to circumnavigate the globe [Robock and Matson, 1983] and was observed to spread vertically between 15 and 35 km over Mauna Loa [De Luisi, 1982]. TOMS was able to track the formation and dispersion of the ash for the first few days after each eruption. The distribution of the TOMS detected ash cloud after the April 4 eruptions, as represented by positive values of the aerosol index, is shown in Figures 2a–2d. In these figures, measurement artifacts such as sea glint, which can be easily determined from geometry, have been removed. The areal coverage of the ash cloud on April 4 (Figure 2a) agrees well with the coverage seen by the GOES satellite, using both visible (0.55–0.75 μ m) and thermal infrared (10.5–12.5 μ m) bands, at approximately the same time [Matson, 1982]. Extensive field studies of ash fall were conducted at 99 locations covering an area of about 45,000 km² [Varekamp *et al.*, 1982]. These studies indicate that ash from the April 4 eruption was deposited primarily in an eastward direction, with the 1-mm isopach at approximately 210 km. These results are consistent with the area of extent determined by TOMS.

While the displacements of both the ash cloud and the SO₂ cloud were roughly the same on April 4, there was a significant geographical separation of the ash cloud from the SO₂ cloud by April 5. The ash cloud itself separated into two clouds, one moving north and one moving south.

The movements of the ash cloud were compared with trajectories calculated from NCEP balanced wind data; the winds were calculated on a 2° latitude by 5° longitude grid. Figures 3a and 3b show the NCEP balanced winds at various altitudes for April 4, 5, and 6. The latitude and longitude of the winds shown are the grid points closest to the center of the two ash clouds. The winds speed and directions indicated in Figure 3a coincide with the movement of the northern cloud, while those in Figure 3b coincide with the southern cloud. Since there was only one ash cloud on April 4, the wind speed and directions for this day are duplicated in Figures 3a and 3b.

As shown in Figure 2a, a strongly positive index was detected by TOMS over the El Chichon eruption site (17.33°N, 93.2°W) on April 4. Because the TOMS measurements were made more than 6 hours after the eruption, a considerable spread of

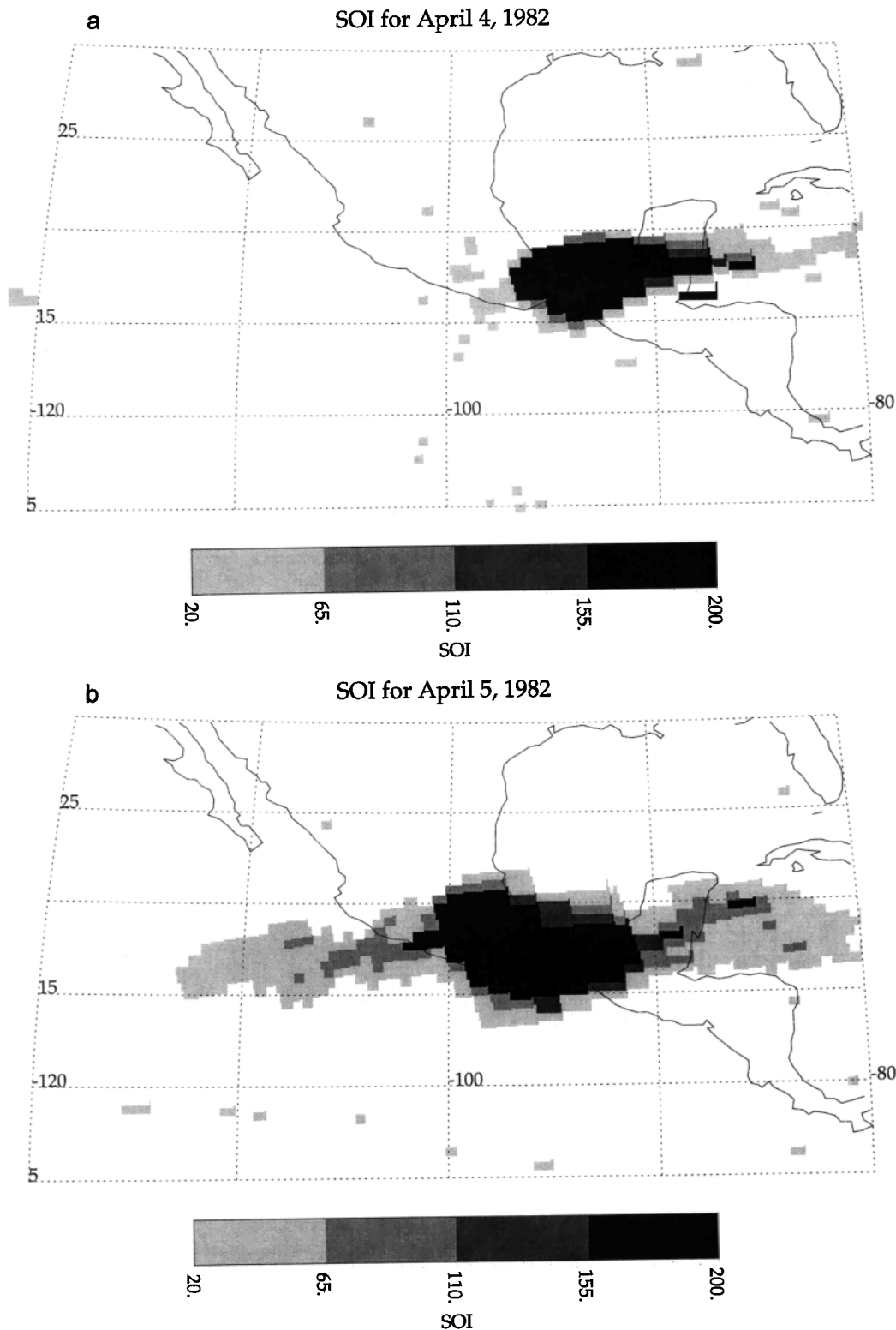


Figure 1. The derived SOI cloud, as seen by TOMS, for (a) April 4, (b) April 5, (c) April 6, and (d) April 8, 1982. April 7 is not shown because a data gap severely limited areal coverage. The areal coverage of each TOMS scan-element measurement is approximated by rectangles; the size of the field of view (and the corresponding rectangle) increases with scan angle.

the ash cloud from the source was observed. The ash cloud was transported in the east-west directions covering most of the area in southern Mexico and northern Guatemala. These motions are consistent with the 1200 UT NCEP balanced wind,

shown in Figure 3a, in the neighborhood of the eruption site and at approximately 70–200 mbar (near the tropopause).

On April 5 (Figure 2b), one section of the ash cloud moved north into the Gulf of Mexico, while the bulk of the ash cloud

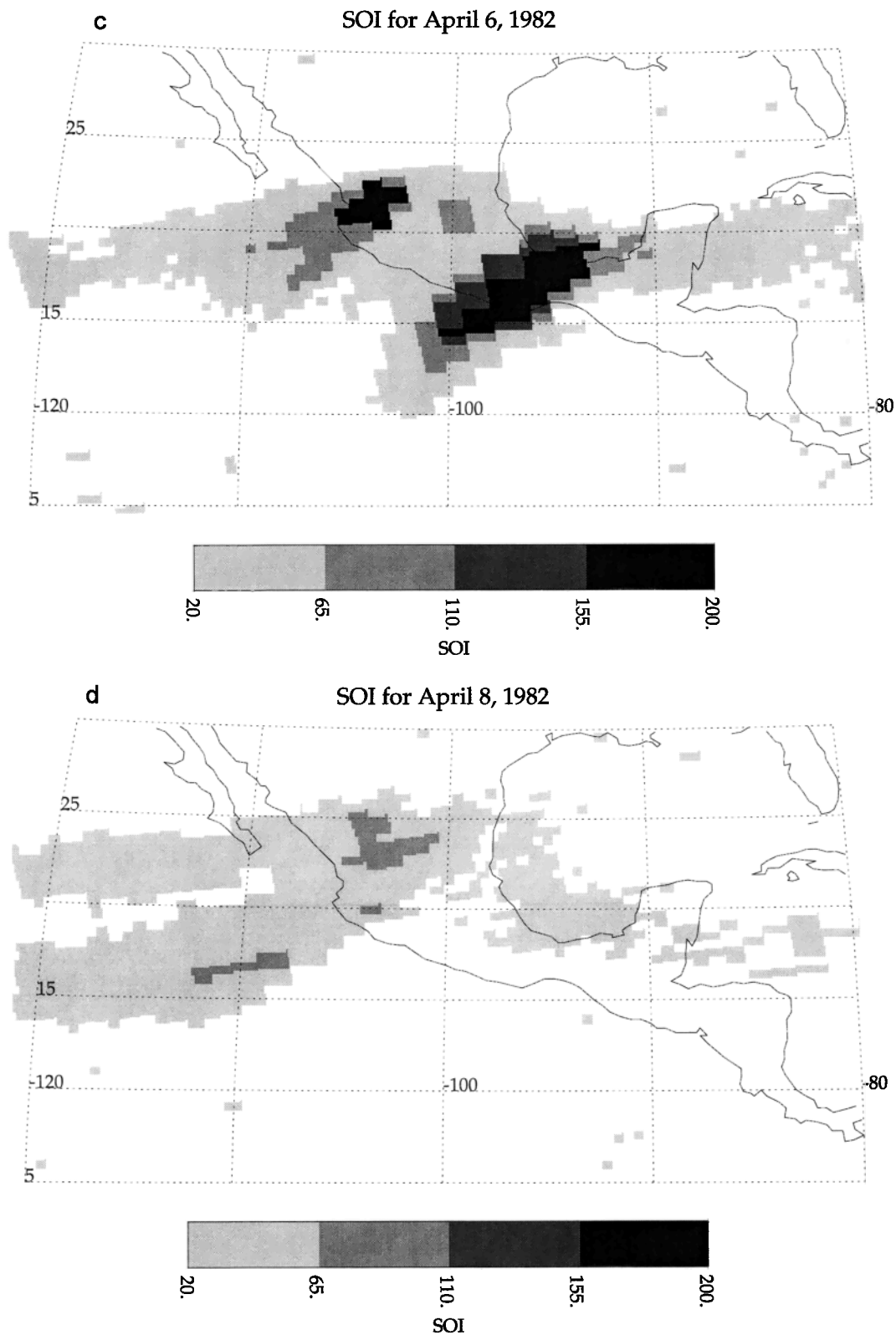


Figure 1. (continued)

drifted slightly to the south. According to the NCEP wind pattern in Figure 3a, the northward movement was only possible in the lower troposphere at an altitude at or below 850 mbar. The tropospheric nature of this cloud is also indicated in

radiosonde data from Veracruz [Matson, 1982; Matson and Robock, 1982]. Reports of a low-altitude (1.5–2 km) cloud were reported blowing over the southern Texas coast on April 5, and a light ashfall occurred in Houston during the night of April 7

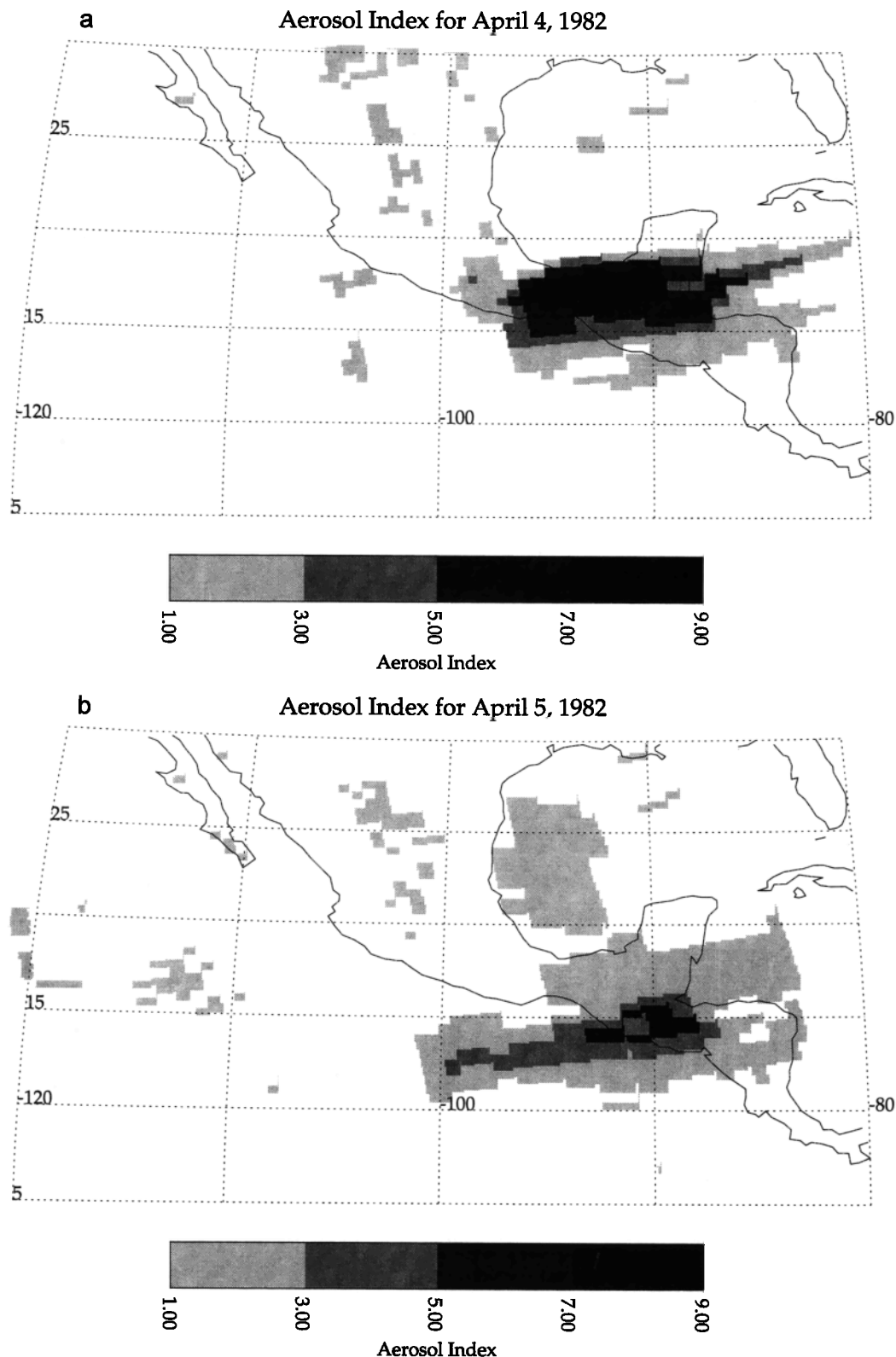


Figure 2. The ash cloud, as seen by TOMS through the calculation of the aerosol index, for (a) April 4, (b) April 5, (c) April 6, and (d) April 8.

[*Smithsonian Institution Scientific Event Alert Network (SEAN)*, 1989]. These reports also indicate that the northern cloud seen by TOMS is contained in the low troposphere.

Figure 3b shows the vertical profile of horizontal wind vec-

tors at 14°N and 90°W on April 5. The weak south-southeast movement of the ash cloud is in agreement with NCEP winds at approximately 50–70 mbar, and Veracruz radiosonde data also indicate that this cloud is stratospheric [Matson, 1982];

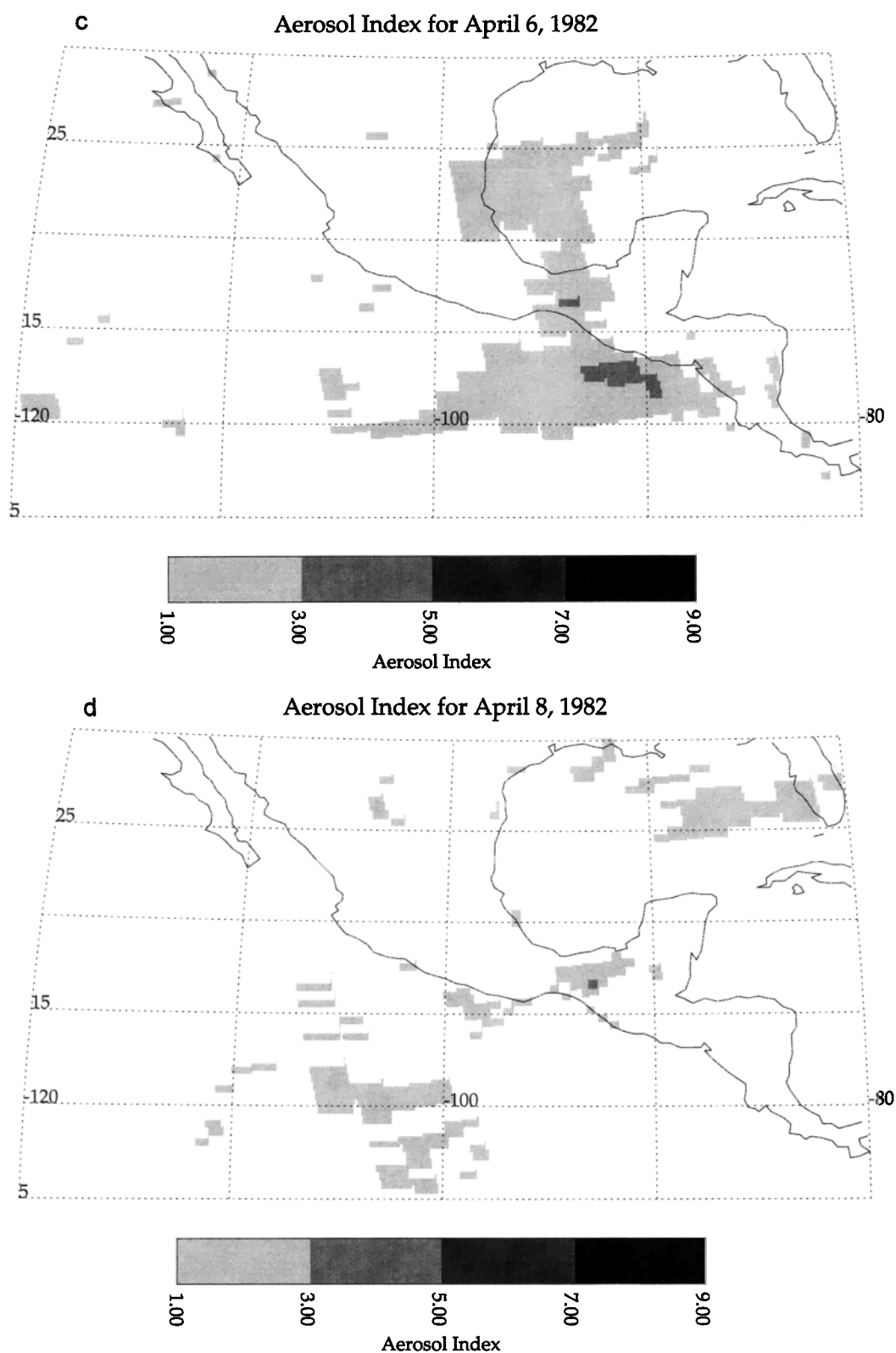


Figure 2. (continued)

the SO_2 cloud follows the NCEP wind pattern at about 10–30 mbar.

On April 6 (Figure 2c) the bulk of the ash cloud detected previously in the Gulf of Mexico on April 5 was still visible and only drifted slightly to the west. Again, this is consistent with

the lower troposphere winds for April 6 depicted in Figure 3a. The bulk of the ash cloud observed in the coastal region near the Pacific Ocean on April 5 moved to the southwest, as seen by TOMS on April 6, again under the influence of stratospheric winds. This ash cloud continued to travel to the west,

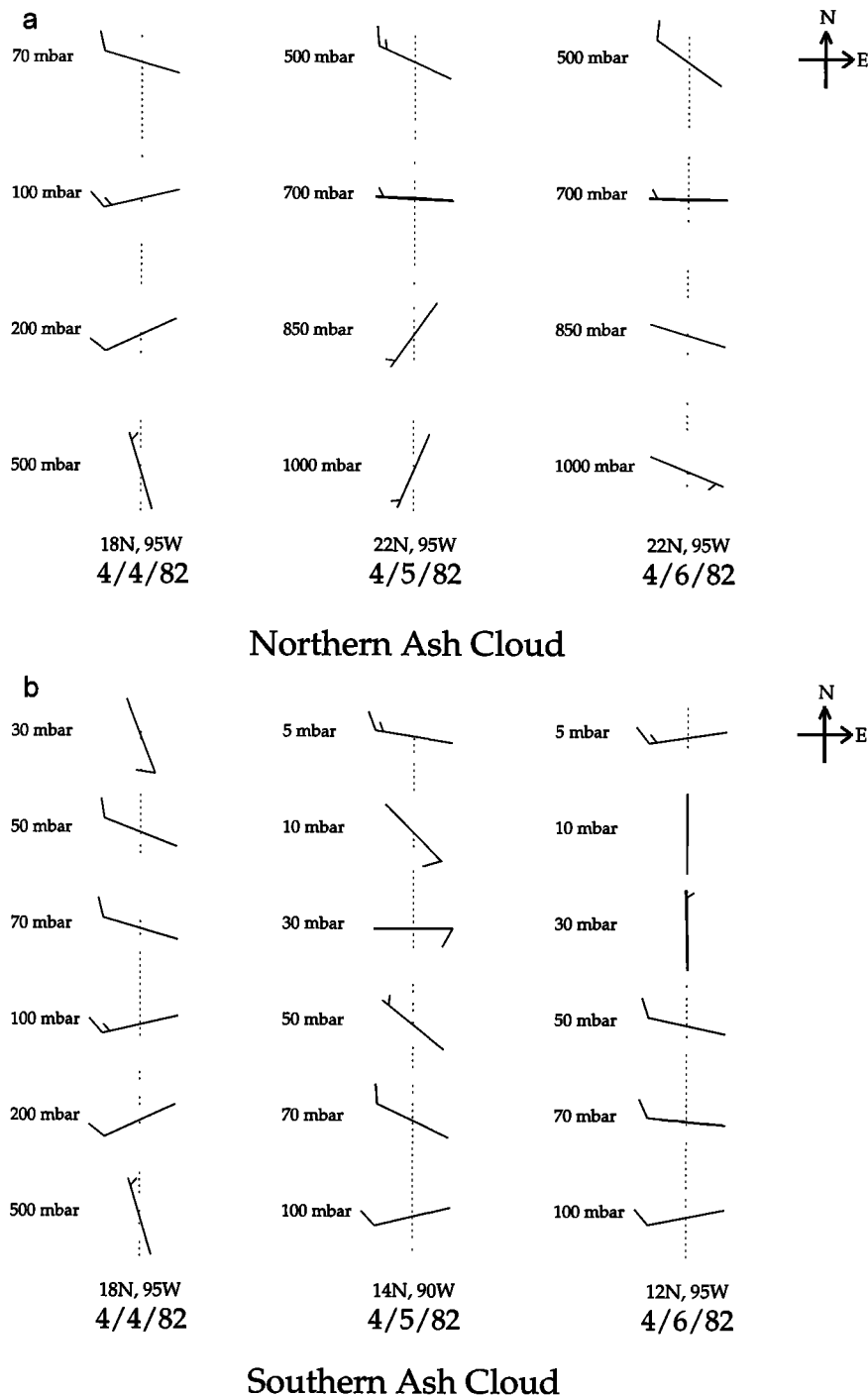


Figure 3. NCEP balanced winds at locations and altitudes consistent with the movement of the (a) northern ash cloud and (b) southern ash cloud.

following the wind circulation in the lower stratosphere on April 7; it then was split by the northerly and southerly flow in the region near 12°N and 98°W, as shown in Figure 2d.

The separation of the ash cloud from the SO₂ cloud for the El Chichon eruption appears to have resulted from the vertical wind shear in the altitude region where the two clouds resided. This separation is consistent with lab experiments performed to study gas-ash separation processes [Holasek *et al.*, 1996].

Data from AVHRR instruments can also be used to detect volcanic ash. If the temperature contrast between the ash cloud

and the surface is large enough, brightness temperatures determined from band 4 (10.3–11.3 μm) and band 5 (11.5–12.5 μm) are used to discriminate volcanic ash clouds from meteorological ones [Wen and Rose, 1994]. These data can be used to retrieve optical depth and effective radius of volcanic ash particles, and ash burdens and mass retrievals can also be performed (D. J. Schneider *et al.*, Observations of sulfur dioxide and volcanic ash in the April 4–7, 1982, El Chichon volcanic cloud as seen with total ozone mapping spectrometer and advanced very high resolution radiometer, submitted to *Jour-*

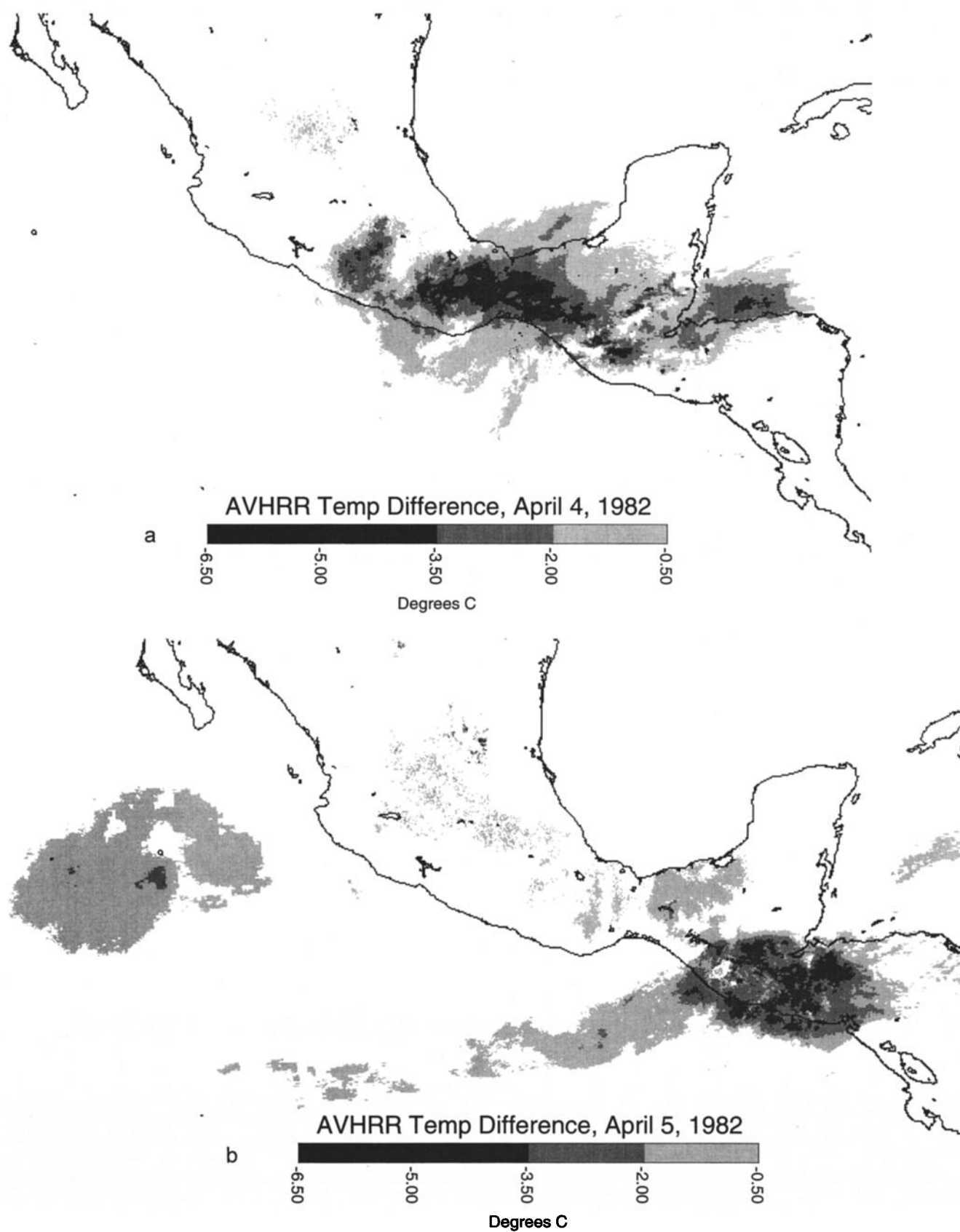


Figure 4. The ash cloud, as seen by AVHRR through the difference in brightness temperature, for (a) April 4, (b) April 5, and (c) April 6. Note the shift in scale in Figure 4c.

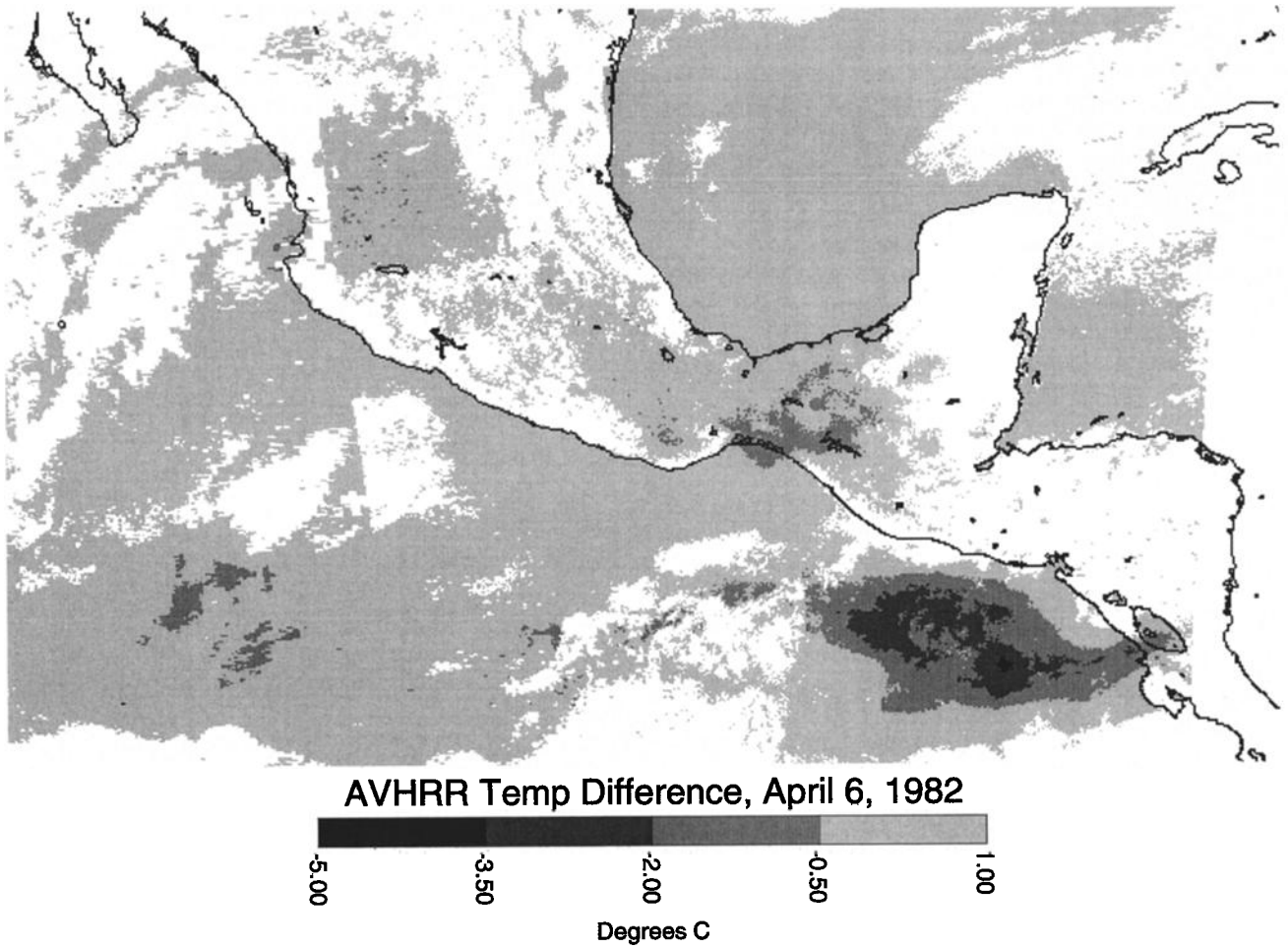


Figure 4. (continued)

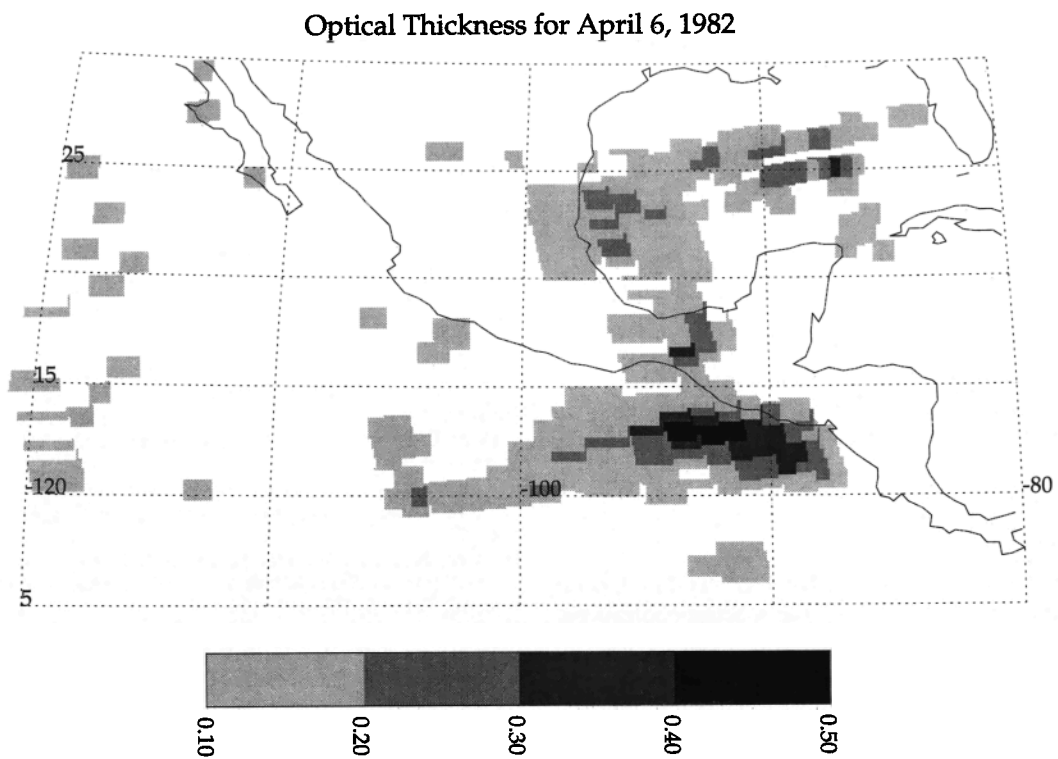


Figure 5. The calculated optical depth calculated for April 6, 1982. The aerosol model used in the radiative transfer calculation is given in the text.

nal of Geophysical Research, 1997) (hereinafter referred to as Schneider et al., submitted manuscript, 1997). For this paper, only the original brightness temperature differences are presented. Figures 4a–4c show the movement of the El Chichon ash cloud as seen by AVHRR on board the NOAA 7 satellite between 2030 and 2230 UT.

The development of the cloud and its movement generally agree with that observed by TOMS. The ash signal detected by the AVHRR in the Gulf of Mexico is very weak and is cut off when converted to mass fraction. This might be due to the fact that the cloud is very low in elevation, leading to a very small temperature contrast between it and the underlying surface.

Many of the differences between the two data sets can be explained by the fact that the AVHRR observations are 2–3 hours later than those from TOMS. An area of disagreement not explained by the time difference exists south of Baja California on April 5. AVHRR detects a sizable area of ash in this area, yet there is no indication of such a cloud from the TOMS measurement. Since the ash burden of this cloud, as determined from the AVHRR measurements (Schneider et al., submitted manuscript, 1997), is an order of magnitude lower than the main cloud to the southeast, the amount of ash is possibly too low for TOMS to detect.

4. Optical Depth for April 6, 1982

The aerosol index observed by TOMS may be converted to optical thickness using radiative transfer calculations provided that an adequate aerosol optical properties model is available. The most critical parameters are the effective radius of the size distribution and the complex index of refraction. Knowledge of the ash vertical distribution and the reflectivity of the underlying surface is also required.

To illustrate the feasibility of deriving ash optical depth from the TOMS measured aerosol index, radiative transfer calculations were carried out using an assumed aerosol model consisting of a polydispersion of silicate ash composed of spherical particles with a lognormal particle size distribution of mode radius (r_0) 1.5μ and width (σ) 1.5. The complex refractive index at 340 and 380 nm was taken to be $1.5-0.0023i$ and $1.5-0.0018i$, respectively, based on reported measurements [Patterson, 1981; Patterson et al., 1983]. The ash vertical distribution is represented by a Gaussian function with a peak at 15 km above sea level (approximately 700 mbar). The derived optical depth is shown in Figure 5. It should be emphasized that the validity of the optical depth derived from this calculation is closely tied to the assumptions of the input aerosol model; any deviations between the actual aerosol properties of the El Chichon ash cloud and those of the aerosol model would lead to differences in the actual optical depth and the one calculated.

5. Conclusion

The Version 7 reprocessing of the Nimbus 7/TOMS data set contains accurate information about the spectral contrast between the 380- and 340-nm channels which can be used to detect absorbing atmospheric particulates. In this work an aerosol index has been defined and used to map and track the motion of the volcanic ash cloud from the April 4, 1982, volcanic eruption of El Chichon. For this eruption the evolution of the ash cloud (until April 8) is presented and shown to be largely consistent with NCEP balanced wind fields and with ash

maps derived from AVHRR. For this volcanic event, TOMS data showed that the ash cloud motions were different from the SO_2 cloud motions due to vertical wind shear. When the data are used in conjunction with information on the optical properties of absorbing particulates (layer altitude, size distribution of the ash, and refractive index), radiative transfer calculations can be used to estimate the ash optical thickness.

Although the current Earth Probe and ADEOS TOMS instruments do not have a 340- or 380-nm wavelength channel, an aerosol index constructed from the spectral contrast between the 331- and 360-nm channels has also been shown to be effective in detecting and tracking absorbing tropospheric aerosols such as volcanic ash.

The use of TOMS radiance measurements to detect both SO_2 and ash clouds not only provides a way of comparing the distribution of gas and ash within an eruption cloud using the same satellite sensor, but the results obtained can be compared to laboratory studies designed to examine the processes in such gas-ash separations [Holasek et al., 1996]. Furthermore, the detection of ash clouds from TOMS complements AVHRR measurements in areas where the temperature contrast between the cloud and the surface is small and AVHRR cannot detect such clouds. Finally, the ability of TOMS to detect the injection of volcanic ash into the atmosphere and to track the motion of the resulting ash cloud during the days following future eruptions will provide useful information for emergency planning as well as for air flight operations [Heffter, 1993].

Acknowledgments. The authors would like to thank the other members of the Ozone Processing Team for their support in generating the Version 7 TOMS data set. We would also like to thank Charlie Schnetzler as well as the reviewer of this manuscript for their helpful comments.

References

- Barth, C. A., R. W. Sanders, R. J. Thomas, G. E. Thomas, B. M. Jakosky, and R. A. West, Formation of the El Chichon aerosol cloud, *Geophys. Res. Lett.*, **10**, 993–996, 1983.
- Bluth, G. J. S., S. D. Doiron, C. C. Schnetzler, A. J. Krueger, and L. S. Walter, Global tracking of the SO_2 clouds from the June, 1991 Mount Pinatubo eruptions, *Geophys. Res. Lett.*, **19**, 151–154, 1992.
- Carey, S. N., and H. Sigurdsson, The 1982 eruption of El Chichon volcano, Mexico, 2, Observations and numerical modeling of tephra-fall distribution, *Bull. Volcanol.*, **48**, 127–141, 1986.
- D'Almeida, G. A., On the variability of desert aerosol radiative characteristics, *J. Geophys. Res.*, **92**, 3017–3026, 1987.
- De Luisi, J., Measurements of the El Chichon dust cloud from Mauna loa observatory, in *Proceedings of the Seventh Annual Climate Diagnostic Workshop*, pp. 383–385, Natl. Oceanic and Atmos. Admin., U.S. Dep. of Commer., Washington, D. C., 1982.
- Heffter, J. L., Volcanic ash forecast transport and dispersion (VAFTAD) model, *Weather Forecasting*, **8**, 533–541, 1993.
- Herman, J. R., P. K. Bhartia, O. Torres, N. C. Hsu, C. J. Seftor, and E. Celerier, Global distribution of absorbing aerosols from Nimbus 7/total ozone mapping spectrometer, data, *J. Geophys. Res.*, in press, 1997.
- Holasek, R. E., A. W. Woods, and S. Self, Experiments on gas-ash separation processes in volcanic umbrella plumes, *J. Volcanol. Geotherm. Res.*, **70**, 169–181, 1996.
- Hsu, N. C., J. R. Herman, P. K. Bhartia, C. J. Seftor, O. Torres, A. M. Thompson, J. F. Gleason, T. F. Eck, and B. N. Holben, Detection of biomass burning smoke from TOMS measurements, *Geophys. Res. Lett.*, **23**, 745–748, 1996.
- Krueger, A. J., Sighting of El Chichon sulphur dioxide clouds with the Nimbus-7 total ozone mapping spectrometer, *Science*, **220**, 1377–1379, 1983.
- Krueger, A. J., L. S. Walter, P. K. Bhartia, C. C. Schnetzler, N. A. Krotkov, I. Sprod, and G. J. S. Bluth, Volcanic sulfur dioxide mea-

- surements from the total ozone mapping spectrometer instruments, *J. Geophys. Res.*, **100**, 14,057–14,076, 1995.
- Matson, M., The 1982 El Chichon volcano eruptions—A satellite perspective, *J. Volcanol. Geotherm. Res.*, **23**, 1–10, 1982.
- Matson, M., and A. Robock, Satellite detection of the 1982 El Chichon eruptions and stratospheric cloud, in *Proceedings of the Seventh Annual Climate Diagnostic Workshop*, pp. 359–370, Natl. Oceanic and Atmos. Admin., U.S. Dep. of Commer., Washington, D. C., 1982.
- McPeters, R. D., et al., Nimbus-7 total ozone mapping spectrometer (TOMS) data products user's guide, *NASA Ref. Publ.*, **1384**, 1996.
- Patterson, E. M., Measurements of the imaginary part of the refractive index between 300 and 700 nanometers for Mt. St. Helens ash, *Science*, **211**, 836–838, 1981.
- Patterson, E. M., and C. K. McMahon, Absorption characteristics of forest fire particulate matter, *Atmos. Environ.*, **18**, 2541–2551, 1984.
- Patterson, E. M., C. O. Pollard, and I. Galindo, Optical properties of the ash from El Chichon volcano, *Geophys. Res. Lett.*, **10**, 317–320, 1983.
- Robock, A., and M. Matson, Circumglobal transport of the El Chichon volcanic dust cloud, *Science*, **221**, 195–197, 1983.
- Seftor, C. J., G. Jaross, J. R. Herman, X. Gu, L. Moy, S. L. Taylor, and C. G. Wellemeyer, The Meteor 3/total ozone mapping spectrometer Version 7 data set: Calibration and analysis, *J. Geophys. Res.*, in press, 1997.
- Sigurdsson, H., S. N. Carey, and J. M. Espindola, The 1982 eruptions of El Chichon, Mexico: Stratigraphy of pyroclastic deposits, *J. Volcanol. Geotherm. Res.*, **23**, 11–37, 1984.
- Smithsonian Institution Scientific Event Alert Network (SEAN), *Global Volcanism 1975–1985*, edited by L. McClelland et al., Prentice-Hall, Englewood Cliffs, N. J., 1989.
- Torres, O., J. R. Herman, P. K. Bhartia, and Z. Ahmad, Properties of Mount Pinatubo aerosols as derived from Nimbus 7 total ozone mapping spectrometer measurements, *J. Geophys. Res.*, **100**, 14,043–14,055, 1995.
- Varekamp, J. C., J. F. Luhr, and K. L. Prestegard, The 1982 eruptions of El Chichon Volcano (Chiapas, Mexico): Character of the eruptions, ash-fall deposits, and gasphase, *J. Volcanol. Geotherm. Res.*, **23**, 39–68, 1982.
- Wellemeyer, C. G., S. L. Taylor, G. Jaross, M. T. Deland, C. J. Seftor, G. Labow, T. J. Swissler, and R. P. Cebula, Final report on Nimbus-7 TOMS Version 7 calibration, *NASA Contract. Rep.*, **4717**, 1996.
- Wen, S., and W. I. Rose, Retrieval of sizes and total masses of particles in volcanic clouds using AVHRR bands 4 and 5, *J. Geophys. Res.*, **99**, 5421–5431, 1994.
- P. K. Bhartia and J. R. Herman, NASA Goddard Space Flight Center, Code 916, Greenbelt, MD 20771.
- N. C. Hsu, N. Krotkov, C. J. Seftor, and O. Torres, Hughes STX Corporation, 7701 Greenbelt Road, Greenbelt, MD 20770. (e-mail: seftor@hoss.stx.com)
- W. I. Rose and D. J. Schneider, Department of Geological Engineering and Sciences, Michigan Technological University, 1400 Townsend Drive, Houghton, MI 49931.

(Received September 18, 1996; revised March 13, 1997; accepted March 26, 1997.)